METALLURGY

Grain boundaries are Brownian ratchets

Caihao Qiu[1], Maik Punke[2], Yuan Tian[3], Ying Han[3], Siqi Wang[1], Yishi Su[4], Marco Salvalaglio[2,5]*, Xiaoqing Pan[3,6]*, David J. Srolovitz[7,8]*, Jian Han[1]*

We demonstrate that grain boundaries (GBs) behave as Brownian ratchets, exhibiting direction-dependent mobilities and unidirectional motion under oscillatory driving forces or cyclic thermal annealing. We observed these phenomena for nearly all nonsymmetric GBs but not for symmetric ones. Our observations build on molecular dynamics and phase-field crystal simulations for a wide range of GB types and driving forces in both bicrystal and polycrystalline microstructures. We corroborate these simulation results through in situ experimental observations. We analyze these results with a Markov chain model and explore the implications of GB ratchet behavior for materials processing and microstructure tailoring.

Kinetic processes in crystalline materials are mediated by the transport of defects (*1*). In particular, the motion of interfaces is the dominant mechanism in grain growth (*2*, *3*), recrystallization (*4*, *5*), first-order phase transformations (*6*, *7*), plastic deformation of nanocrystalline materials (*8*, *9*), and polarization switching in ferroic materials (*10*, *11*). Application of (configurational) forces drives the motion of an interface in one direction (*12*, *13*). The potential for unidirectional interface motion without a driving force is motivated by the observation that grain growth can be accelerated by oscillatory variation of homogeneous temperature or stress fields (*14*–*16*). Understanding how these nondriven migrations occur and their implications is of fundamental interest.

Although nondriven transport is not rare in nature, it has rarely been recognized for interfaces. In a noninterface context, one notable example is the molecular motor (*17*, *18*), where some biomolecules subjected to nonequilibrium fluctuations move (or rotate) in one direction (*19*). These unidirectional transport phenomena under random perturbations are often described as Brownian ratchets (*20*–*22*). We demonstrate that most interfaces in crystalline materials are natural Brownian ratchets, exhibiting unidirectional motion when subjected to a fluctuating field. This finding holds important implications for grain boundary (GB) engineering and materials processing.

[1]Department of Materials Science and Engineering, City University of Hong Kong, Hong Kong, China. [2]Institute of Scientific Computing, TU Dresden, 01062 Dresden, Germany. [3]Department of Materials Science and Engineering, University of California, Irvine, CA 92697, USA. [4]State Key Laboratory of Metal Matrix Composites, School of Materials Science and Engineering, Shanghai Jiao Tong University, Shanghai 200240, China. [5]Dresden Center for Computational Materials Science, TU Dresden, 01062 Dresden, Germany. [6]Irvine Materials Research Institute (IMRI), University of California, Irvine, CA 92697, USA. [7]Department of Mechanical Engineering, The University of Hong Kong, Hong Kong, China. [8]Materials Innovation Institute for Life Sciences and Energy (MILES), The University of Hong Kong, Shenzhen, China.
*Corresponding author. Email: jianhan@cityu.edu.hk (J.H.); srol@hku.hk (D.J.S.); marco.salvalaglio@tu-dresden.de (M.S.); xiaoqinp@uci.edu (X.P.)

Directional GB migration

We focus on GBs, a common class of homophase interfaces. We demonstrate that the mobilities of typical nonsymmetric GBs in different materials and with different tilt axes depend on the direction (or sense) of the driving force. We conducted molecular dynamics (MD) simulations in which we drive GB migration by creating a free energy density jump (ψ) across the GB (arising from anisotropy in elastic constant, excess defect density, and magnetic anisotropy) (*13*) or by applying a stress (τ) tangential to the GB (*12*) [see section 1 in (*23*)]. In particular, we examine Σ27 [110] asymmetric tilt GB (ATGB) in Cu driven by ψ (Fig. 1A), Σ11 [110] ATGB in Al driven by ψ (Fig. 1B), Σ19 [110] ATGB in Al driven by ψ (Fig. 1C), Σ99 [110] symmetric tilt GB (STGB) in Cu driven by τ (Fig. 1D), and Σ25 [100] ATGB in Al driven by τ (Fig. 1E) (see the simulation settings in table S1). In each case, the GB is driven by forces of at least three different values; each simulation is repeated at least three times (see all data in fig. S2). Once a GB normal $\mathbf{n}$ is chosen, the signs of ψ and τ are well defined. We denote the GB migration rate as the absolute value of the GB velocity $v_{+/-}$, where +/− indicates positive/negative driving forces (Fig. 1, A to E). These data clearly demonstrate that $|v_+| \neq |v_-|$—i.e., the GB migration rates under positive and negative driving forces are different. The actual driving forces are obtained by thermodynamic integrations and are provided in table S2.

We reveal the origin of directional migration by examining the structures of the migrating GBs. The common feature in all these cases is that the atomic structure of the migrating GBs is different when they migrate in opposite directions. The Σ27 ATGB (Fig. 1F) dissociates into a twin boundary and another GB when it migrates in one direction while remaining undissociated when migration is in the opposite direction. Migration of the Σ11 ATGB (Fig. 1G) is dominated by the motion of one single set of facets when it migrates in one direction and by the motion of two distinct sets of facets in the other. Migration of the Σ19 ATGB (Fig. 1H) is controlled by the motion of different sets of facets when it migrates in opposite directions. Although the Σ99 STGB (Fig. 1I) is symmetric from the point of view of bicrystallography, this GB exhibits a 9R phase, which is microscopically nonsymmetric—the width of the 9R phase is different when it migrates in different directions. The Σ25 low-angle ATGB (Fig. 1J) migrates through the glide of different sets of GB dislocations when it migrates in opposite directions. The change in the GB migration mechanism under opposite driving forces can also be probed by the change in the shear-coupling factor (fig. S15). We find that directional GB migration involves dissociation of the GB into two types of constituent defects (e.g., dissociation into two sets of facets or two low-energy boundaries). Two distinct sets of constituent defect structures correspond to two distinct energy barriers. The apparent GB mobility depends on the mechanism by which defect motion drives GB migration, further determined by the nature of the GB structural asymmetry relative to the direction of the driving force. Directional GB migration has been observed in the experiments by Molodov *et al.* (*24*) on magnetically driven GB migration in bismuth bicrystals and in the MD simulations by McCarthy and Rupert (*25*) on synthetic force–driven migration of Σ11 GBs in various metals. The directional GB migration observed in these simulations was attributed to preferential emission of stacking faults on one side of the GB, which is similar to our Σ99 case.

Although we examined five GB migration cases as detailed above, we conducted additional MD simulations for a series of GBs for which no structural dissociation occurs (*26*, *27*) to showcase the generality of our observation. GB geometry is described by five macroscopic degrees of freedom (DOFs)—tilt axis $\mathbf{o}$ (2 DOFs), rotation angle θ (1 DOF), and GB normal $\mathbf{n}$ (2 DOFs) (*28*). If $\mathbf{n} \perp \mathbf{o}$ and the two grains are symmetry related, the GB is an STGB (Fig. 2A). The two grains can be related by a mirror plane m' with normal $\mathbf{n}$ and/or a 2′-fold rotation axis parallel to $\mathbf{p} \equiv \mathbf{n} \times \mathbf{o}$ (where prime indicates the operations that transform one grain to another). For the Σ39 STGB of our concern, both m' and 2′ exist. Tilting the STGB plane about the $\mathbf{o}$ axis with an angle $\phi_{\mathbf{o}}$ yields an ATGB (Fig. 2B). Tilting the STGB plane about the $\mathbf{p}$ axis with an angle $\phi_{\mathbf{p}}$ yields a symmetric mixed GB (SMGB) (Fig. 2C)—in constructing a SMGB, the 2′ axis is preserved. Tilting the STGB plane about an axis lying in the GB plane but different from $\mathbf{p}$ yields an

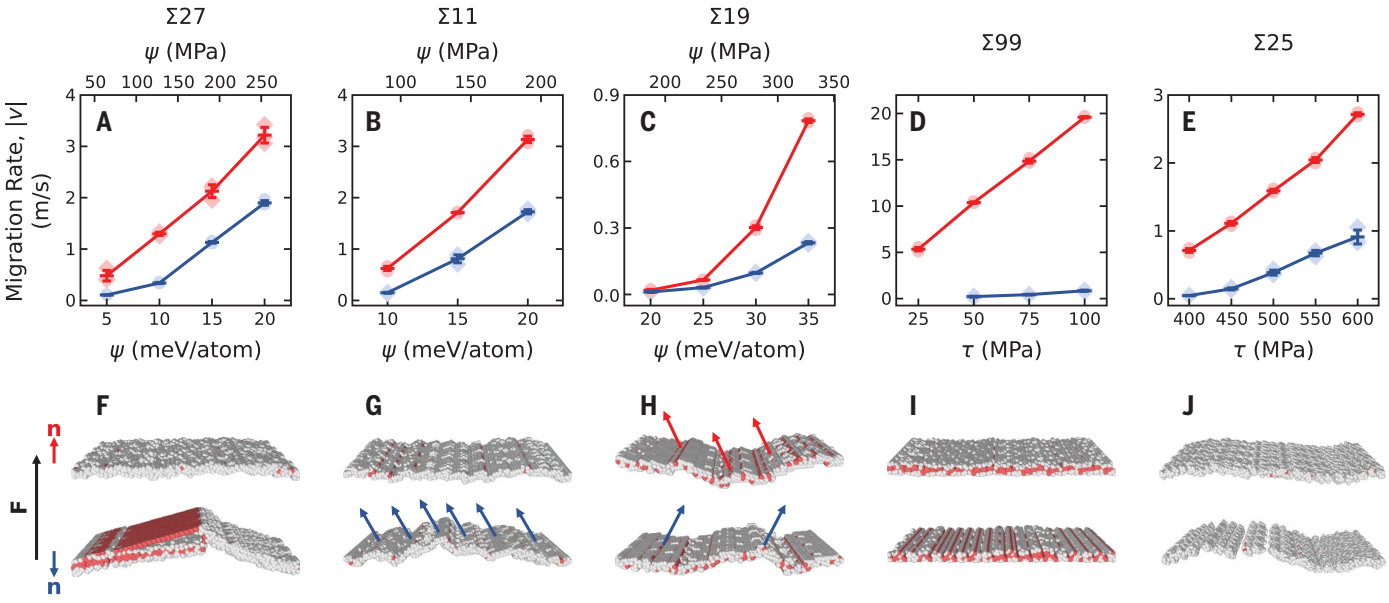

Fig. 1. GB migration under driving forces in opposite directions. The GBs include Σ27 [110] ATGB [(A) and (F)], Σ11 [110] ATGB [(B) and (G)], Σ19 [110] ATGB [(C) and (H)], Σ99 [110] STGB [(D) and (I)], and Σ25 [100] ATGB [(E) and (J)]. (**A** to **E**) GB migration rates versus driving forces (ψ or τ). GB velocities are always in the same sense as the driving forces. Light red circles and light blue diamonds show the data for each individual simulation for positive ($F = \mathbf{F}\cdot\mathbf{n} > 0$) and negative ($F < 0$) driving forces, respectively. The short horizontal bars denote the means and standard deviations. (**F** to **J**) Structures of migrating GBs under positive and negative driving forces (upper and lower panels, respectively). The atoms with a local perfect crystal environment are not shown, and red atoms are locally hexagonal close packed.

asymmetric mixed GB (AMGB) (Fig. 2D). No symmetry relationship exists between the two grains adjacent to ATGBs or AMGBs. We show (Fig. 2, F to I) the ratio of the GB migration rates $|v_+/v_-|$ for different ψ for a set of Σ39 [111] GBs—i.e., STGB, ATGB ($\phi_\mathbf{o} = 9.8°$), SMGB ($\phi_\mathbf{p} = 36.3°$), and AMGB (equivalent to combining $\phi_\mathbf{o} = 9.8°$ and $\phi_\mathbf{p} = 36.3°$). All the simulations were performed at $0.5T_\mathrm{m}$ (where T_m is the melting point) six times with different initial conditions. We find that $|v_+/v_-| > 1$ for the ATGB and AMGB (Fig. 2, G and I, and fig. S5) in every individual simulation. On the other hand, the STGB and SMGB show $|v_+/v_-| = 1$ within the standard deviation of the individual simulation data (Fig. 2, F and H). These results demonstrate, with a high level of statistical significance, that the mobilities of STGB and SMGB are independent of the direction of the driving force. From the MD simulation results (Fig. 2), we can conclude that if the two grains adjacent to the GB are not symmetry related, then the migration mobilities depend on the direction of the driving force. If the migration mobility is independent of the direction of the driving force, then the two grains meeting at the GB must be symmetry related. We briefly return to the case of Fig. 1D, showing that an STGB exhibits direction-dependent GB mobility. Although macroscopically this GB is symmetric, the interfaces between the grains and the 9R domain are not (there is a sense to the 9R structure). Simulations run over a long time period should show equal probability of each sense such that, on average, even this GB should exhibit direction-independent GB mobility.

In real, polycrystalline microstructures, GBs are generally curved (inclination angle is not constant) and are mainly driven by capillarity (curvature flow). Consider the GB half-loop configuration in Fig. 2E, where the GB is curved and yet migrates at a constant rate (*29*). We investigate both cases where the crystal of the blue/brown orientations are on the outside/inside of the half-loop. So, the sense of the capillary force driving GB migration relative to the normal is reversed, whereas the spectra of GB type along the half-loops in the two cases are identical (fig. S8). We show (Fig. 2J and fig. S7) that the migration rates in these two cases are unequal ($|v_+/v_-| \neq 1$, and the migration for the lower panel in Fig. 2E is always larger than that for the upper panel) for all GB curvatures studied at $0.7T_\mathrm{m}$ (curvature is $1/w$). From this, we conclude that even in capillarity-driven GB migration, the GB mobility depends on the driving force direction. Overall, we see that directional GB mobility is irrelevant to whether the GB is flat or curved or the origin of the driving force for migration.

Markov chain analysis

An infinitely large, flat GB cannot migrate as a whole. Instead, it migrates by the nucleation and expansion of disconnection loops, where disconnections are line defects constrained to interfaces and have both step and dislocation character (*30*, *31*). We show two-dimensional (2D) analogs of this—i.e., nucleation of a pair of disconnections separated by upward and downward terraces on both an STGB and ATGB (Fig. 3, A and B). On STGBs, the upward and downward terrace configurations are related by mirror and 2′-fold symmetries (Fig. 3A). Both the disconnection structures (denoted by the red segments in Fig. 3A) and the disconnection glide events (indicated by the gray and yellow shaded, striped areas in Fig. 3A) involved in upward and downward GB migration are identical. However, for an ATGB, the upward and downward terraces are not symmetry related (Fig. 3B). The upward terrace grows by the glide of the red/green disconnection through the gray/yellow shaded area, whereas the downward terrace grows by the glide of the green/red disconnection through the blue/red shaded area. For the ATGB case, moving a disconnection (red or green segment in Fig. 3B) in opposite directions is nonequivalent and occurs at different rates.

We validate these assertions by determining the minimum energy paths (MEPs) for the nucleation, propagation, and annihilation of a disconnection pair. We determined the motions of the $\Sigma11[110](1\bar{1}3)$ STGB and ATGB (with $\phi_\mathbf{o} = 46.7°$ studied in Fig. 1B) in Al [section 3 in (*23*) and Fig. 3, C and D]. The MEP for the STGB is symmetric about the midpoint

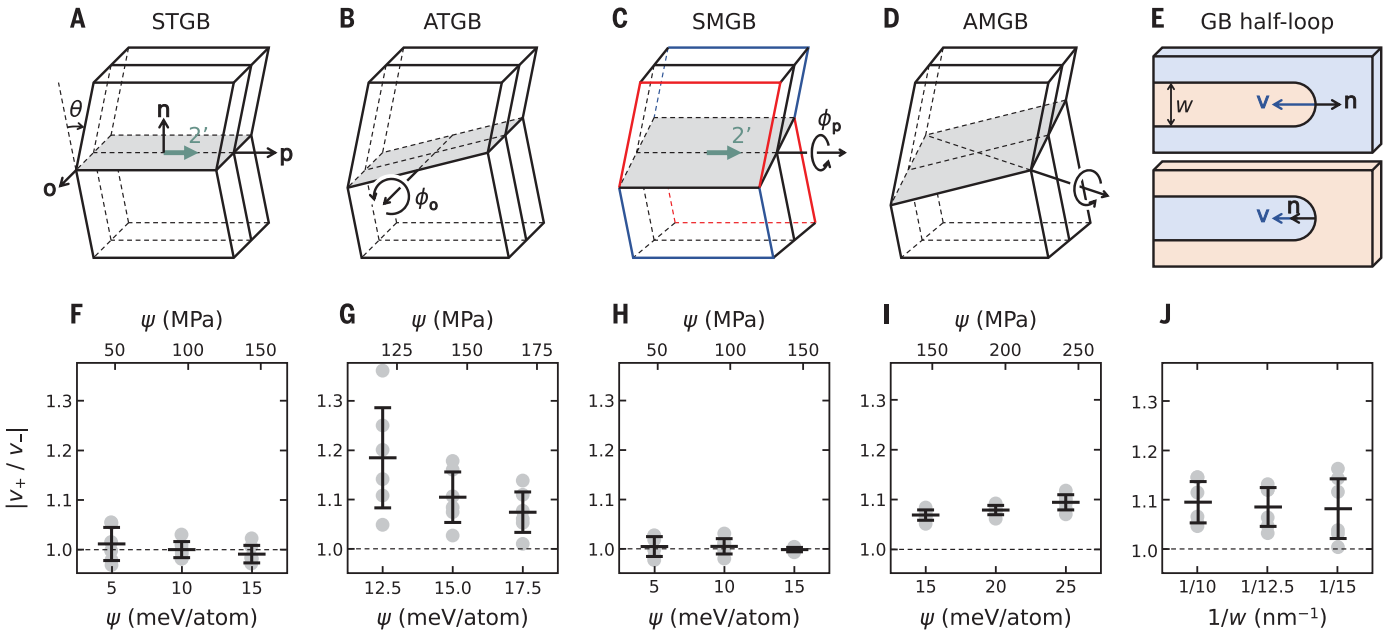

Fig. 2. Comparison of GB migration rates under opposite driving forces. The bicrystal configurations include STGB [(A) and (F)], ATGB [(B) and (G)], SMGB [(C) and (H)], AMGB [(D) and (I)], and GB half-loop [(E) and (J)]. (**A** to **E**) Schematics of bicrystal constructions and the symmetries relating two grains (2′-fold axis). In (E), the brown and blue regions indicate grains of two different orientations. (**F** to **J**) Ratios between the GB migration rate ratio for two directions $|v_+/v_-|$ versus driving forces, ψ, or curvature, $1/w$, obtained from the MD results for Σ39 flat GBs and Σ13 GB half-loops in Al. Six simulations were performed for each GB at each ψ. The gray points show individual simulation results, and the black symbols represent the mean values and standard deviations of the data.

of the path (Fig. 3C), whereas that for the ATGB is nonsymmetric (Fig. 3D). The supercell for the ATGB simulation contains two GB structure periods (details in fig. S12D). To describe the migration of the same GB (STGB or ATGB) in the opposite direction, we can use the same MEP and flip it about the midpoint between the initial and final states.

To illustrate the consequences of a symmetric versus nonsymmetric MEP for GB migration, we first idealize the MEPs (Fig. 3, E and F). We envision these MEPs as representing the motion of a "GB" from one atomic plane "a" to an adjacent and equivalent plane "a" through a metastable state "b." We evolve the system along the Markov chain (Fig. 3G), for which we determined the transition probabilities according to the transition state theory [section 4 in (*23*)]. The simulation leads to an evolving probability distribution (for where the "GB" sits), $P(i,t)$, at state i along the chain and step (time) t. In the absence of a driving force, F, the distribution P is a Gaussian with a standard deviation growing as t. The same result applies to both symmetric and nonsymmetric MEPs. However, when a force is applied, the Gaussian spreads, and the mean "GB" position (in the sense of ensemble average) moves in the direction of the force at a rate that depends on the force magnitude. For the symmetric MEP case (Fig. 3E), the "GB" migration rate (from the peak positions at different times) is independent of the sign of F (Fig. 3H). On the other hand, when the MEP is nonsymmetric (Fig. 3F), the "GB" migration rate is larger for $F > 0$ than $F < 0$ (Fig. 3I). Our Markov chain analysis demonstrates that a nonsymmetric MEP is a necessary condition for directional "GB" migration (special nonsymmetric MEPs exist for which "GB" migration is force direction independent; fig. S18).

Because the MD simulations and Markov chain analysis both show that the GB migration rate depends on the sign of driving force, the application of an oscillatory zero-mean driving force should give rise to unidirectional GB migration. To consider this effect within the Markov chain approach, we apply an oscillatory driving force of the form $F_t = (-1)^{\lfloor ft \rfloor}\Delta F$, where f is the frequency, ΔF is the amplitude of the driving force oscillation, and $\lfloor ft \rfloor$ represents the integer part of ft. As seen in Fig. 3J for the "STGB" (symmetric MEP), the mean "GB" does not move with an oscillatory driving force (zero net velocity). However, the "ATGB" (nonsymmetric MEP) moves to the right at a constant rate in the presence of an oscillatory force (Fig. 3K). The forcing frequency has much less influence on the so-called migration rate than the oscillatory forcing amplitude (Fig. 3K, inset).

In a more general context, unidirectional motion in response to oscillatory forcing is a common feature of Brownian ratchets (*20*–*22*). Hence, we may classify GBs as Brownian ratchets. In fact, both GBs and Brownian ratchets can be described in terms of the same type of Markov chain with nonsymmetric MEPs. In this regard, GBs and Brownian ratchets are "isomorphic." An exceptional Brownian ratchet behavior is unidirectional motion in response to cyclic annealing (*21*) (fig. S20). This motivates us to examine the GB–Brownian ratchet analogy by exposing the "GB" to an oscillatory temperature of the form $T_t = \bar{T} + (-1)^{\lfloor ft \rfloor}\Delta T$, where $\bar{T}$ and ΔT are the mean temperature and the temperature oscillation range. The results are shown in Fig. 3, L and M, for the "STGB" and "ATGB" (symmetric and nonsymmetric MEPs). In the symmetric MEP case (STGB), the "GB" moves to neither the right nor the left, whereas in the nonsymmetric MEP case (ATGB), the "GB" moves to the right at a constant rate. The "ATGB" migration rate increases with increasing temperature cycling frequency; at a fixed frequency, the migration rate increases with increasing temperature cycling amplitude before reaching a maximum at $\Delta T/\bar{T} \approx 0.8$ (Fig. 3M, inset).

Unidirectional GB migration under oscillatory loading

Our analysis of the GB Brownian ratchet behavior was based on a simplified Markov chain model. To determine whether it applies to real GBs, we conducted MD simulations on the migration of the Σ39 [111] STGB and ATGB (the GBs in Fig. 2, A and B) under both oscillatory ψ and τ driving forces at $0.6T_m$. Here, $\psi = 15 \times (-1)^{\lfloor ft \rfloor}$ (in milli–electron volts per

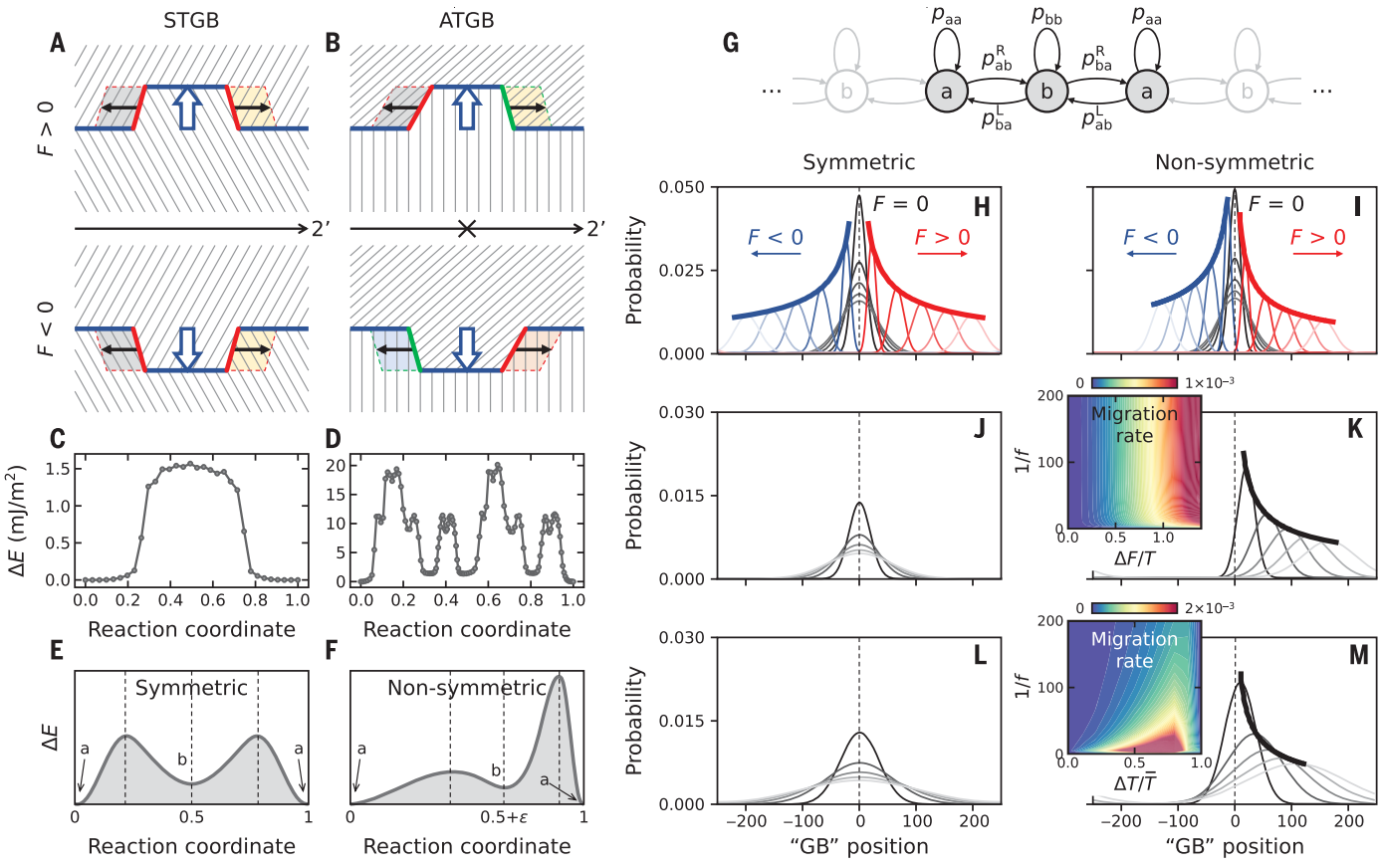

Fig. 3. Explanation of directional GB motion. (**A** and **B**) Illustrations of the nucleation and growth of upward and downward terraces on an STGB and ATGB. The hollow blue arrows denote the direction of GB migration, and the short black arrows denote the direction of disconnection motion. The blue line segments represent GB terraces, and the red and green line segments represent the disconnections of different types. The gray stripes indicate equivalent crystal planes. The shaded parallelograms denote regions swept by the disconnections during GB migration. The parallelograms (including the gray stripes) that are not related by symmetry (e.g., 2′) are shaded in different colors. (**C** and **D**) MEPs for Σ11 [110] STGB and ATGB in Al. (**E** and **F**) Representations of the MEPs of (C) and (D), consistent with their symmetries. (**G**) A Markov chain labeled with the transition probabilities $\{p_{ij}\}$ [see the labels "a" and "b" in (E) and (F)]. (**H** to **M**) Evolutions of state probability distributions; (H), (J), and (L) are obtained based on the symmetric MEP (E), whereas (I), (K), and (M) are for the nonsymmetric model (F). (H and I) Probability distribution evolution under no (black), positive (red), and negative (blue) driving forces. (J and K) Results for oscillatory change in driving force. (L and M) Cyclic annealing. The insets of (K) and (M) show the GB migration rate as a function of the driving force and the temperature oscillation frequency and amplitude, respectively.

atom) or $\tau = 150 \times (-1)^{\lfloor ft \rfloor}$ (in megapascals), where $f = 1\ \mathrm{ns}^{-1}$ (Fig. 4, A to D). For the STGB, the GB position fluctuates on oscillatory loading, and on average, the GB velocity is zero. For the ATGB, although the GB position still fluctuates on oscillatory loading, the GB drifts with a constant, unidirectional mean velocity of ~0.45 m/s for ψ and ~0.16 m/s for τ. This velocity for oscillatory ψ is consistent with $||v_+| - |v_-|| \times 10 = 0.523 \pm 0.204$ m/s that we obtained from the data in Fig. 2G.

We also examined the effect of periodic cycling of the annealing temperature using the phase-field crystal (PFC) method (*32*, *33*), which provides access to much longer simulation times than are accessible with MD simulations (*34*, *35*) [section 2 in (*23*)]. We obtained results for the STGB and ATGB by the PFC method with a temperature cycling frequency of $3.7 \times 10^3\ \mathrm{s}^{-1}$ (the absolute value of the temperature is a phenomenological parameter in PFC; table S4) (Fig. 4, E and F). As with the oscillatory driving forces, under cyclic annealing, the STGB does not migrate, whereas the ATGB exhibits a constant, unidirectional velocity of ~1.5×10^{-8} m/s. The PFC results for long-time GB processes (in 0.5 s) are shown in movies S1 and S2.

We present an in situ scanning transmission electron microscopy (STEM) observation of the unidirectional migration of an ATGB in a Ni bicrystal sample (Fig. 4G) under annealing with constant and oscillatory temperatures [section 5 in (*23*)]. The upper grain is on the zone axis close to [112], whereas the lower grain is close to [110]; so, the GB is nonsymmetric. The sample was initially annealed at 400°C for 20 min. The GB migrated at a negligible rate (0.08 ± 0.05 nm/min) (light gray region in Fig. 4H). From 20 to 129 min, the sample underwent cyclic annealing between 350° and 450°C with a frequency of 0.33 Hz. The GB migrated in one direction (Fig. 4G and brown region of Fig. 4H) at a rate 5.61 ± 0.32 nm/min. From 129 to 157 min, the sample was annealed at a constant high temperature (450°C). The GB migrated at a small rate (1.32 ± 0.06 nm/min). The slight GB migration observed under constant temperature annealing is likely driven by the surface energy difference of the two grains. The large GB migration rate observed during cyclic annealing cannot be explained by the surface effect but can back up the Brownian ratchet mechanism revealed by our simulations and analysis.

Implications for microstructure tailoring

Polycrystalline materials are commonly used for technological applications, so how the GB Brownian ratchet effect influences the

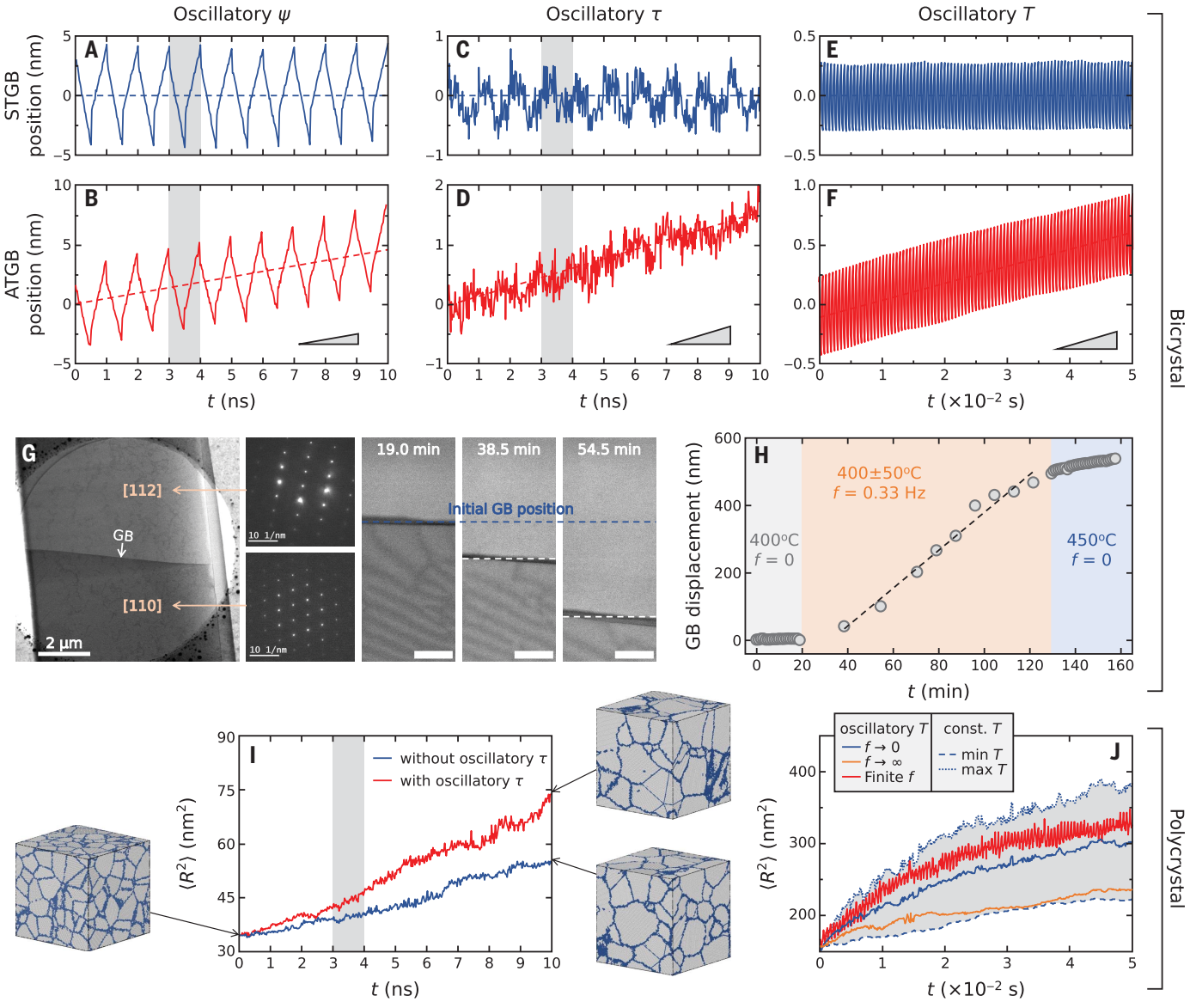

Fig. 4. Demonstrations of the GB Brownian ratchet. (**A** and **B**) Evolutions of mean position of the Σ39 [111] STGB (blue) and ATGB (red) in Al under an oscillatory synthetic driving force. (**C** and **D**) Displacements of the same GBs under oscillatory shear stress. (A) to (D) are MD results. The gray shading indicates one loading period. (**E** and **F**) Displacements of the same GBs under cyclic annealing obtained from PFC simulations. The long-time results are shown in movies S1 and S2. (**G**) Bicrystal sample for in situ STEM observation of GB migration. The diffraction patterns show that the zone axis is [112] for the upper grain and [110] for the lower grain. The snapshots (scale bars, 40 nm) at 20, 30, and 40 min are given, where the blue and white dashed lines indicate the initial and current GB positions. (**H**) GB displacement versus time. In the light gray and blue regions, the sample is annealed at 400° and 450°C, respectively. In the brown region, cyclic annealing is performed between 350° and 450°C with a frequency of 0.33 Hz; the dashed line is a linear fitting of the data in this region. (**I**) MD results for grain growth in a 3D polycrystalline Al, including the atomic structures at t = 0 and 10 ns (where the GB atoms are colored blue) and the mean squared grain size versus time with oscillatory τ (red) and with τ = 0 (blue). (**J**) PFC results for the mean squared grain size in a 2D polycrystalline Al versus time with cyclic thermal annealing (red), constant high (blue dotted curve), low (blue dashed curve) and mean (orange solid curve) temperatures, and the average of the high- and low-temperature results (blue solid curve).

microstructure evolution is of broad practical interest. We conjecture that applying an oscillatory driving force or nonequilibrium thermal fluctuations will lead to the unidirectional drift of most GBs. Unidirectional GB drift will accelerate grain growth or shrinkage in a polycrystal, either of which contributes to an increase in the net growth of the mean grain size.

To investigate this, we performed MD simulations of grain growth in polycrystalline Al at $0.6T_m$ under an oscillatory shear stress with zero mean, stress amplitude well below the yield strength, and an oscillation frequency of 1.0 ns^{-1}. In these simulations, we observed no substantial dislocation plasticity or twinning (Fig. 4I). We compared the evolution of the mean squared grain size $\langle R^2 \rangle$ obtained from our MD simulation with (red curve) and without (blue curve) an oscillatory shear stress (Fig. 4I). We found that the mean grain growth rate $\langle dR^2/dt \rangle$ is ~2 times as high in the presence of an oscillatory shear stress. Notably, a few experimental observations exist of grain growth acceleration under oscillatory loading [i.e.,

tension-compression (*14*, *16*) or bending (*36*, *37*)]. These observations are phenomenologically consistent with the MD results and our suggestion—based on the GB–Brownian ratchet analogy—that grain growth is accelerated by applying an oscillatory driving force.

We also performed PFC simulations to show that cyclic annealing accelerates grain growth, as the GB–Brownian ratchet analogy suggests. We compared the evolution of grain size in the simulation with (red curve) and without (blue and orange curves) a cyclic temperature variation (Fig. 4J). The dotted and dashed blue curves show the results for grain growth under the constant high and low temperatures, corresponding to the maximum and minimum values of the temperature oscillation. The solid blue curve is the average of these two curves, mimicking the limiting case of cyclic annealing with frequency $f \to 0$. The solid orange curve is the result of grain growth at the mean temperature, equivalent to the result for cyclic annealing with $f \to \infty$. By comparing the solid blue and orange curves with the red curve, we find that cyclic annealing at a finite frequency accelerates grain growth. The maximum growth rate will occur at a certain finite frequency. The above PFC results are also presented in movies S3 to S6.

There has been extensive literature over the past several decades that suggests that diverse oscillatory fields (thermal, mechanical, electrical, magnetic, etc.) can enhance the grain growth rate by up to 1500% and the recrystallization rate by up to 300%; these findings are summarized in table S6. These effects have been attributed to the reduction in activation energy for grain growth. However, the mechanism by which the activation energy reduction arises from the oscillation in the fields remains unclear. We show that the Brownian ratchet model provides an explanation for this mechanism.

Given the observed directional dependency of GB mobility, it is important to revise the classical kinetic equation for GB motion—i.e., $v = MF$, where v is the GB velocity, F is the driving force, and M is the GB mobility. Once we reverse the direction of the driving force—i.e., $F \to -F$—the classical equation predicts that the GB velocity becomes $-v$, which is inconsistent with our analysis, MD simulations, and several experimental observations. This issue can be resolved by modifying the mobility to make it a function of the sign of F—i.e., $M(F/|F|)$. In addition, the velocity of nonsymmetric GBs should, as a general rule, be nonzero when the driving force F is oscillatory (even when the mean force $\bar{F} = 0$) and/or the temperature T is cycled. The equation for GB motion may be empirically rewritten in the form $v = M\bar{F} + \alpha(\Omega\Delta F/k_B\bar{T}) + \beta e^{-\gamma/f_T}(\Delta T/\bar{T})$, where M is a function of the sign of the mean driving force $\bar{F}/|\bar{F}|$ and the mean temperature $\bar{T}$; ΔF and ΔT are the amplitudes of the driving force and temperature oscillations; f_T is the cyclic annealing frequency; Ω is the atomic volume; k_B is the Boltzmann constant; and α, β, and γ are parameters that are functions of temperature, material, and GB structure. Such a modified equation for GB motion incorporates steady and oscillatory driving forces and cyclic annealing effects. This expression may be used in any phenomenological model for microstructure evolution with assumed (or measured) values of the parameters, allowing for more realistic descriptions of GB motion as well as a guide for designing thermomechanical processing to manipulate microstructures.

The implication of direction-dependent GB mobility and the effects of oscillatory fields are potentially important for interpreting experimental observations of GB motion in a polycrystal and for simulating microstructure evolution. Specifically, microstructure evolution simulations should not assume that the mobility of a GB is constant [a conclusion reached by others but for other reasons (*38*)] nor that mobilities can be correctly extracted from experiments by monitoring averaged mobilities. For example, the direction of GB motion during microstructure evolution may switch as a result of the topological change in microstructure, and the direction-averaged mobility has no physical meaning.

REFERENCES AND NOTES

1. A. Kelly, K. M. Knowles, *Crystallography and Crystal Defects* (Wiley, ed. 3, 2020).
2. M. Hillert, *Acta Metall.* **13**, 227–238 (1965).
3. E. A. Holm, S. M. Foiles, *Science* **328**, 1138–1141 (2010).
4. F. J. Humphreys, M. Hatherly, *Recrystallization and Related Annealing Phenomena* (Elsevier, 1995).
5. S. Schmidt *et al*., *Science* **305**, 229–232 (2004).
6. J. W. Christian, *The Theory of Transformations in Metals and Alloys* (Elsevier, ed. 3, 2002).
7. Y. Peng *et al*., *Nat. Mater.* **14**, 101–108 (2015).
8. K. Lu, L. Lu, S. Suresh, *Science* **324**, 349–352 (2009).
9. L. Liu *et al*., *Science* **368**, 1347–1352 (2020).
10. C. T. Nelson *et al*., *Science* **334**, 968–971 (2011).
11. D. Pantel, S. Goetze, D. Hesse, M. Alexe, *Nat. Mater.* **11**, 289–293 (2012).
12. J. W. Cahn, Y. Mishin, A. Suzuki, *Acta Mater.* **54**, 4953–4975 (2006).
13. K. G. Janssens *et al*., *Nat. Mater.* **5**, 124–127 (2006).
14. H. W. Höppel, Z. M. Zhou, H. Mughrabi, R. Z. Valiev, *Philos. Mag. A* **82**, 1781–1794 (2002).
15. S. S. Sahay, C. P. Malhotra, A. M. Kolkhede, *Acta Mater.* **51**, 339–346 (2003).
16. P. Zhao *et al*., *Acta Mater.* **174**, 29–42 (2019).
17. R. D. Vale, R. A. Milligan, *Science* **288**, 88–95 (2000).
18. M. Schliwa, G. Woehlke, *Nature* **422**, 759–765 (2003).
19. P. Reimann, *Phys. Rep.* **361**, 57–265 (2002).
20. R. P. Feynman, R. B. Leighton, M. Sands, *The Feynman Lectures on Physics, Volume 1: Mainly Mechanics, Radiation, and Heat* (Addison-Wesley, ed. 2, 2005).
21. R. D. Astumian, *Science* **276**, 917–922 (1997).
22. P. Illien, O. Bénichou, G. Oshanin, A. Sarracino, R. Voituriez, *Phys. Rev. Lett.* **120**, 200606 (2018).
23. Materials and methods are available as supplementary materials online.
24. D. Molodov, G. Gottstein, F. Heringhaus, L. Shvindlerman, *Scr. Mater.* **37**, 1207–1213 (1997).
25. M. J. McCarthy, T. J. Rupert, *Phys. Rev. Mater.* **4**, 113402 (2020).
26. S. L. Thomas, K. Chen, J. Han, P. K. Purohit, D. J. Srolovitz, *Nat. Commun.* **8**, 1764 (2017).
27. E. R. Homer, S. M. Foiles, E. A. Holm, D. L. Olmsted, *Acta Mater.* **61**, 1048–1060 (2013).
28. A. P. Sutton, R. W. Balluffi, *Interfaces in Crystalline Materials* (Oxford Univ. Press, 2007).
29. G. Gottstein, L. S. Shvindlerman, *Grain Boundary Migration in Metals: Thermodynamics, Kinetics, Applications* (CRC Press, ed. 2, 2010).
30. J. Han, S. L. Thomas, D. J. Srolovitz, *Prog. Mater. Sci.* **98**, 386–476 (2018).
31. Q. Zhu *et al*., *Nat. Commun.* **10**, 156 (2019).
32. K. R. Elder, M. Katakowski, M. Haataja, M. Grant, *Phys. Rev. Lett.* **88**, 245701 (2002).
33. V. Skogvoll, M. Salvalaglio, L. Angheluta, *Model. Simul. Mater. Sci. Eng.* **30**, 084002 (2022).
34. H. Emmerich *et al*., *Adv. Phys.* **61**, 665–743 (2012).
35. Z. Trautt, A. Adland, A. Karma, Y. Mishin, *Acta Mater.* **60**, 6528–6546 (2012).
36. B. L. Boyce, H. A. PadillaII, *Metall. Mater. Trans. A* **42**, 1793–1804 (2011).
37. J. Yang *et al*., *Mater. Sci. Eng. A* **839**, 142875 (2022).
38. J. Zhang *et al*., *Acta Mater.* **191**, 211–220 (2020).
39. C. Qiu *et al*., Multi-scale Simulation Data to Prove that Grain boundaries are Brownian ratchets, version 9, Dryad (2024); https://doi.org/10.5061/dryad.0k6djhb8v.

ACKNOWLEDGMENTS

Funding: This study was supported by the National Key R&D Program of China 2021YFA1200202 (J.H.); the National Key R&D Program of China 2022YFB3708900 (Y.S.); the Early Career Scheme (ECS) grant from the Hong Kong Research Grants Council CityU21213921 (J.H.); the Army Research Office (ARO) under grant W911NF-19-1-0263 (X.P.); the Hong Kong Research Grants Council General Research Fund 17210723 (D.J.S.); Deutsche Forschungsgemeinschaft (DFG, German Research Foundation), project no. 447241406 (M.P. and M.S.); and the National Natural Science Foundation of China 51971132 and 52192595 (Y.S.). M.P. and M.S. acknowledge the computing time made available to them on the high-performance computer at the National High Performance Computing (NHR) Center of TU Dresden, project "p_crystal." **Author contributions:** Conceptualization: J.H. and D.J.S. Methodology: C.Q., M.P., Y.T., Y.H., S.W., M.S., D.J.S., and J.H. Formal analysis: C.Q., M.P., Y.T., M.S., D.J.S., and J.H. Validation: C.Q., M.P., Y.T., Y.H., M.S., and J.H. Resources: M.S., X.P., D.J.S., J.H., and Y.S. Software: C.Q., M.S., M.P., S.W., and J.H. Supervision: J.H., D.J.S., and M.S. Writing – original draft: C.Q. and J.H. Writing – review & editing: Y.S., M.S., M.P., X.P., D.J.S., and J.H. **Competing interests:** The authors declare that they have no competing interests. **Data and materials availability:** All data are available in the main text, the supplementary materials, Dryad (*39*), and GitLab (https://gitlab.com/3ms-group/directional-migration.git).

SUPPLEMENTARY MATERIALS

science.org/doi/10.1126/science.adp1516
Materials and Methods
Supplementary Text
Figs. S1 to S21
Tables S1 to S6
References (*40*–*66*)
Movies S1 to S6

Submitted 13 March 2024; accepted 19 July 2024
10.1126/science.adp1516